Frustrated magnets without geometrical frustration in bosonic flux ladders

Letter

Frustrated magnets without geometrical frustration in bosonic flux ladders

Luca Barbiero [1,*] Josep Cabedo [2,*,†] Maciej Lewenstein [3,4] Leticia Tarruell [3,4] and Alessio Celi [2]

[1]*Institute for Condensed Matter Physics and Complex Systems, DISAT, Politecnico di Torino, I-10129 Torino, Italy*

[2]*Departament de Física, Universitat Autónoma de Barcelona, E-08193 Bellaterra, Spain*

[3]*ICFO - Institut de Ciencies Fotoniques, The Barcelona Institute of Science and Technology, Avenida Carl Friedrich Gauss 3, E-08860 Castelldefels (Barcelona), Spain*

[4]*ICREA, Passeig de Lluís Companys 23, E-08010 Barcelona, Spain*

(Received 22 December 2022; revised 7 August 2023; accepted 14 September 2023; published 6 October 2023)

We propose a scheme to realize a frustrated Bose-Hubbard model with ultracold atoms in an optical lattice that comprises the frustrated spin-1/2 quantum *XX* model. Our approach is based on a square ladder of magnetic flux $\sim\pi$ with one real and one synthetic spin dimension. Although this system does not have geometrical frustration, we show that at low energies it maps into an effective triangular ladder with staggered fluxes for specific values of the synthetic tunneling. We numerically investigate its rich phase diagram and show that it contains bond-ordered-wave and chiral superfluid phases. Our scheme gives access to minimal instances of frustrated magnets without the need for real geometrical frustration, in a setup of minimal experimental complexity.

DOI: 10.1103/PhysRevResearch.5.L042008

Introduction. The interplay between geometrical frustration and quantum fluctuations leads to exotic states of matter such as resonating valence bond and quantum spin-liquid phases [1–3]. The simplest models encompassing the richness of frustrated quantum magnets are antiferromagnetic Heisenberg Hamiltonians on triangular lattices [4], which include deconfined quantum critical points [5–7], anyonic liquids [8], and where spontaneous dimerization and chiral order appear [9–13]. In this Letter, we focus on a minimal instance of the frustrated antiferromagnetic Heisenberg model, the spin-1/2 quantum *XX* model on a triangular two-leg ladder. We show that its rich phase diagram can be effectively accessed with ultracold bosons in flux ladders of square lattice geometry, a setup of minimal experimental complexity that is routinely realized with real-space [14,15] and synthetic dimension approaches [16–24].

While the investigation of spin-1/2 Heisenberg triangular ladder systems in solid state materials is a very active field of research [25–31], the broad tunability of ultracold atoms offers an attractive alternative to investigate magnetic frustration in a pristine setting and gives access to new observables. On the one hand, Fermi gases in triangular optical lattices or optical tweezer arrays provide ideal implementations of the celebrated J_1-J_2 antiferromagnetic Heisenberg Hamiltonian [32–34], although achieving experimental temperatures below the superexchange energy scale remains a formidable challenge [35,36]. On the other hand, strongly interacting bosonic systems subjected to artificial magnetic fluxes also display frustrated magnetic phases, but at larger (and accessible) energy scales set by the tunneling [37,38]. However, despite tremendous progress in the realization of artificial gauge fields in such systems using real-space lattices [14,15,39–43], the combination of large magnetic fluxes and strong interactions leads to detrimental heating processes that hinder the investigation of quantum magnetism [44].

An alternative approach, more resilient to heating, is to employ semisynthetic flux ladders with one fictitious dimension constituted by internal spin states coupled via two-photon Raman transitions [16,45], a system that has been successfully employed to experimentally investigate few-leg square ladder systems in both noninteracting [17–20] and strongly interacting regimes [24], but is not straightforward to generalize to triangular geometries without introducing additional heating mechanisms [46,47]. In this Letter, we propose a scheme to realize a frustrated quantum spin model—inbuilt in a semisynthetic flux ladder—*without the need for explicit geometrical frustration*. Building on our previous work [48], we exploit an analytical map between the square flux ladder at low energies and a triangular system with staggered magnetic fluxes. Related schemes have been very recently proposed in fermionic synthetic ladders [49,50], although no effective frustration was investigated in this setting. Here, we identify parameter regimes where the effective geometric frustration plays an important role at accessible temperatures, numerically show that the system displays the same ground state phases as the frustrated spin-1/2 quantum *XX* model [51], and identify suitable observables to reveal them in current experiments with ultracold atoms.

Model. We consider the two-leg semisynthetic bosonic flux ladder [16] in the translation-invariant gauge-transformed

*These authors contributed equally to this work.

†josep.cabedo@uab.cat

frame [52] [see Fig. 1(a)],

$$H_{\square} = \sum_{j,\sigma}\left(-te^{-\imath\gamma\sigma}a^{\dagger}_{j+1,\sigma} + \frac{\Omega}{4}a^{\dagger}_{j,-\sigma} + \frac{\delta}{2}\sigma a^{\dagger}_{j,\sigma}\right)a_{j,\sigma} + \text{H.c.} + \sum_{j,\sigma}\left(\frac{U_{\sigma,\sigma}}{2}n_{j,\sigma}(n_{j,\sigma}-1) + \frac{U_{\sigma,-\sigma}}{2}n_{j,\sigma}n_{j,-\sigma}\right). \quad (1)$$

Here, $a^{\dagger}_{i\sigma}$ ($a_{i\sigma}$) creates (annihilates) a boson in site i of a one-dimensional (1D) optical lattice of length L—we restrict ourselves to 1D systems throughout this Letter—and two different internal atomic states $\sigma = \pm 1/2$ coupled via Raman transitions realize the two legs of the ladder. The intraleg tunneling t is the conventional tunneling rate along the lattice, while the interleg tunneling amplitude is proportional to the Raman Rabi frequency Ω. The two-photon Raman detuning yields a potential interleg offset δ, and a classical magnetic flux γ results from the momentum transfer of the Raman beams. Atoms experience intraleg on-site and interleg nearest-neighbor interactions, which we choose to be identical $U_{\sigma,\sigma} = U_{\sigma,-\sigma} = U$. The total atom number is $N = \sum_{i=1}^{L}\sum_{\sigma} n_{i,\sigma}$, with $n_{i,\sigma} = a^{\dagger}_{i,\sigma}a_{i,\sigma}$ the density in site i.

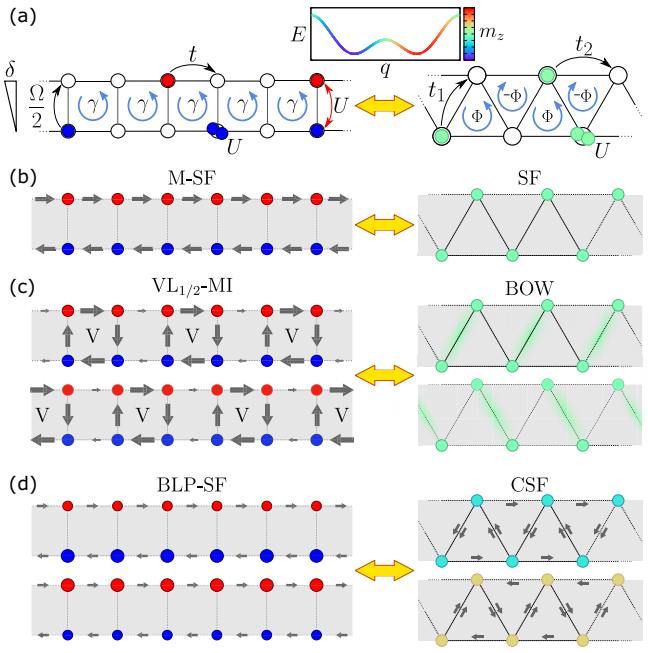

FIG. 1. Mapping semisynthetic square ladders into frustrated triangular ladders. (a) Left: Original square flux-ladder model (1), with intra- and interleg tunnelings t and $\Omega/2$, interleg offset δ, on- and off-site interactions U, and magnetic flux γ. Right: Truncated lower-band Hamiltonian (2), describing an effective triangular ladder with complex tunnelings t_1 and t_2, on-site interactions U, and staggered flux Φ. Inset: Single-particle dispersion relation of the lower-energy band of the square flux ladder for strong Ω and $\gamma \sim \pi$. (b)–(d) Current (arrow) and density (circle) patterns of the flux-ladder phases at average density $\rho = 1/4$ (left), and corresponding phases of the effective triangular model at half filling (right). (b) Meissner superfluid (M-SF): Superfluid (SF) of the triangular model. (c) Vortex lattice insulator ($VL_{1/2}$-MI): Bond-ordered wave (BOW). (d) Biased-ladder superfluid phase (BLP): Chiral superfluid (CSF). Circles and arrows in the square ladder sketches are scaled according to their numerical values at $\Omega = 10t$ and $\delta = 0$, with γ and U adjusted so that $t_2/|t_1| = 0.2$ in (b), $t_2/|t_1| = 0.5$ in (c), and $t_2/|t_1| = 1.0$ in (d), and $U = 10|t_1|$. The BLP is signaled by the difference of circle size between both legs. Color scale: Spin composition m_z of the ground states in the semisynthetic ladder.

In the strong Raman coupling limit $\Omega \gg t$, the two single-particle dispersion bands of (1) are separated by an energy gap $\sim\Omega$ [52]; we denote them as lower- and higher-band dressed states. When the condition $\Omega \gg U$ is also fulfilled, the low-energy properties of the system are captured by a Hamiltonian that includes only lower-band modes,

$$H_{\triangle} = \sum_{l=1,2} t_l \sum_i (b^{\dagger}_i b_{i+l} + \text{H.c.}) + \frac{U}{2}\sum_i \tilde{n}_i(\tilde{n}_i - 1), \quad (2)$$

where $b^{\dagger}_j$ (b_j) are the bosonic creation (annihilation) operators for the inverse-Fourier-transformed lower-band dressed states and $\tilde{n}_j = b^{\dagger}_j b_j$ [see Supplemental Material (SM) [52] for the derivation]. In this regime, the effective Hamiltonian (2) describes a system of N bosons in a lattice of length L with the same on-site interaction U but with effective nearest-neighbor (NN) t_1 and next-nearest-neighbor (NNN) t_2 complex tunnelings. It is thus equivalent to a triangular ladder with staggered magnetic flux $\Phi = \pi - 2\delta\tan(\gamma/2)/\Omega + \mathcal{O}[(\delta/\Omega)^2]$ [see Fig. 1(a)]. At $\delta = 0$, the staggered flux ladder is fully frustrated with $\Phi = \pi$. To order $\mathcal{O}[(t/\Omega)^2]$, the effective tunneling amplitudes in $H_{\triangle}$ relate to the parameters of $H_{\square}$ by [52]

$$t_1 \simeq -t\cos(\gamma/2) \quad \text{and} \quad t_2 \simeq t^2\sin^2(\gamma/2)/\Omega. \quad (3)$$

In the ultracold atom context, the triangular Bose-Hubbard ladder Hamiltonian (2) has been mainly studied at unity filling [61–63] and low densities [64] (for nonstaggered fluxes, see Ref. [65]). Moreover, detailed studies of the hard-core boson (HCB) limit ($U \to \infty$) at half filling $N/L = 1/2$ and flux $\phi = \pi$, where the system is further mapped to a frustrated spin-1/2 quantum XX model ($b^{\dagger}_i, b_j \to S^{+}_i, S^{-}_j$, see SM [52]) have been performed [51,66,67]. In this regime, a gapless superfluid (SF) is found at low values of $|t_2/t_1|$, signaled by the power-law decay of the one-body correlator $g^1(|i-j|) = \langle b^{\dagger}_i b_j\rangle$. At intermediate values of $|t_2/t_1|$, a gapped translation-breaking bond-ordered-wave (BOW) phase is stabilized [see Fig. 1(c)]. It is signaled by nonzero values of the two-point operator $O_{\text{BO}} = \sum_i[(-1)^i/L](b^{\dagger}_i b_{i+1} + b_i b^{\dagger}_{i+1})$. Its insulating nature is signaled by the exponential decay of $g^1(|i-j|)$ and by a finite charge gap $\Delta_c = E_{L,N+1} + E_{L,N-1} - 2E_{L,N}$, computed from the extrapolated ground state energies at $N = L/2$. Finally, for larger $|t_2/t_1|$, a gapless chiral superfluid (CSF) phase emerges. There, the system presents two nonequivalent minima in the dispersion relation, and interatomic interactions favor the occupation of either of the two minima. This degeneracy yields two solutions that spontaneously break a Z_2 parity symmetry [see Fig. 1(d)], and exhibit a finite chirality

$k_i = 2\imath(b_i b_{i+1}^\dagger - b_i^\dagger b_{i+1})$. Thus, the chiral correlation function $k^2(|i-j|) = \langle k_i k_j \rangle$ identifies the CSF.

In our realization of the triangular model (2), we can widely adjust the ratio $|t_2/t_1|$ while arbitrarily approaching the HCB limit within the effective model by setting $|t_{1,2}| \ll U \ll \Omega$. Therefore, we expect that at filling $\rho = 1/4$ the flux ladder Hamiltonian (1) reproduces the whole phase diagram of the quantum XX model with the order parameters written in terms of the currents and densities of the undressed bosons, and that the phases are experimentally accessible [52].

The SF phase of the triangular model translates into the Meissner superfluid phase (M-SF) of the flux ladder [68] [see Fig. 1(b)], characterized by vanishing rung currents and off-diagonal quasi-long-range order. The BOW phase corresponds to a vortex lattice insulating phase ($VL_{1/2}$-MI) of maximal vortex filling $\rho_v = 1/2$, where the effective dimers correspond to the vortex plaquettes [see Fig. 1(c)]. The nature of the BOW phase in the bare basis is easily understood from the susceptibility of the energy against the explicit dimerization of the leg tunnelings [52], through which one can identify

$$O_{\mathrm{BO}} \simeq \sum_{j,\sigma} \frac{2(-1)^j \,\mathrm{Re}(te^{-\imath\gamma\sigma} a_{j+1,\sigma}^\dagger a_{j,\sigma})}{Lt\cos(\gamma/2)}. \tag{4}$$

The BOW phase is characterized by the staggered current patterns of the vortices, and is signaled by the staggered leg current

$$j_{sl} = \frac{1}{L}\sum_{j,\sigma} 4\sigma(-1)^j \,\mathrm{Im}(te^{-\imath\gamma\sigma} a_{j+1,\sigma}^\dagger a_{j,\sigma}), \tag{5}$$

together with the exponential decay of the one-body correlator. Finally, the CSF corresponds to a biased-ladder superfluid phase (BLP-SF), characterized by a spontaneous density imbalance between both legs of the ladder [69,70] [see Fig. 1(c)]. Around $\delta = 0$,

$$k_j \simeq -\frac{2\Omega}{t\sin(\gamma/2)} m_z^{(j)}, \tag{6}$$

where $m_z^{(j)} = \sum_\sigma \sigma a_{j,\sigma}^\dagger a_{j,\sigma}$ is the magnetization or the interleg population imbalance at site j [52].

Based on these correspondences, we propose to detect the different phases by measuring the response of the system to the explicit breaking of the Z_2 parity and translation symmetries of the Hamiltonian. The former is easily achieved by setting the Raman detuning δ to nonzero values. The latter can be implemented by a spatial modulation of the optical lattice using superlattice potentials to dimerize the lattice structure, parametrized by including in (1) a position-dependent tunneling strength $t_j = t(1 + \Delta(-1)^j)$ between sites j and $j+1$. In this way, the spontaneous breaking of the Z_2 symmetry of the ground state in the CSF (or BLP-SF) phase is signaled by the discontinuity in the mean magnetization $\langle m_z \rangle = \frac{1}{N}\sum_j \langle m_z^{(j)} \rangle$ around $\delta = 0$. Similarly, the spontaneous dimerization of the BOW (or $V_{1/2}$-MI) phase is signaled by the jump of the staggered currents (5) around $\Delta = 0$.

Numerical results. To assess the predictions of the effective model (2), we run density-matrix-renormalization-group (DMRG) [71,72] simulations of Hamiltonian (1) in the regimes discussed. In Fig. 2(a), we show the values of Δ_c, O_{BO}, and k^2 as a function of $|t_1/t_2|$, for the ground states of both the effective triangular Hamiltonian (2) at half filling (triangles) and the original square ladder Hamiltonian (1) at filling $\rho = 1/4$ (squares). For the latter, we set $\Omega = 20t$, use (3) to retrieve the corresponding values of t_2 and t_1, and use expressions (4) and (6) to compute O_{BO} and k^2. In both cases, the interaction strength is set to $U = 10t\cos(\gamma/2) = 10|t_1|$, which realizes the strongly interacting regime of the effective triangular ladder. We observe very good agreement between both models in this regime of parameters. Moreover, the phase diagram predicted in the HCB limit of the effective model [51] is preserved for large but finite values of $U/|t_1|$ and Ω. The gapless SF (M-SF) phase appears for sufficiently low $|t_2/t_1|$. For higher values of $|t_2/t_1|$ the quasi-long-range order is lost and a phase with gap $\Delta_c \neq 0$ occurs instead. It is captured by finite values of O_{BO}, signaling the dimerization that characterizes the BOW phase of the triangular model, or, equivalently, the vortex structures of the $V_{1/2}$-MI phase in the square ladder [see (4)]. Finally, a gapless phase analogous

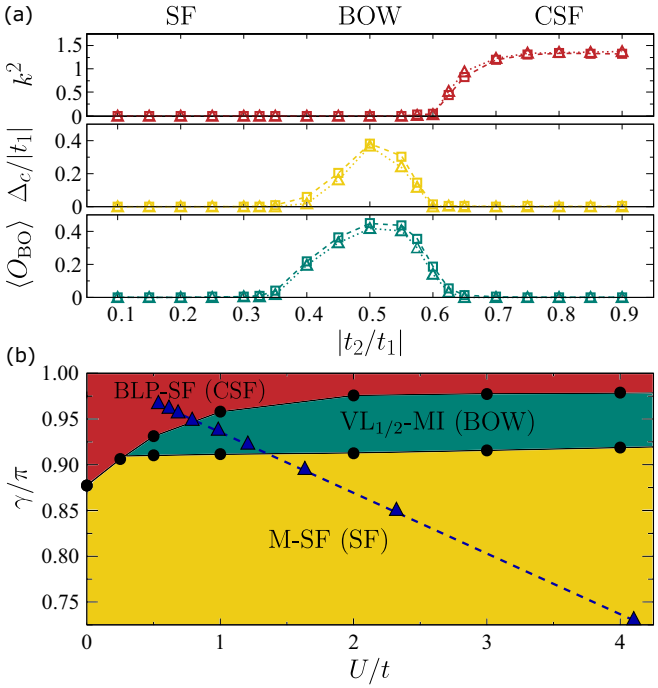

FIG. 2. Phase diagram. (a) DMRG-computed values of chiral correlation function $k^2(L/2)$ (top panel), charge gap Δ_c (central panel), and two-point bond-order operator O_{BO} (bottom panel) as a function of $|t_2/t_1|$ extrapolated to $L \to \infty$. Triangles: Effective triangular staggered-flux ladder (2) at half filling, with $U = 10|t_1|$ and $\Phi = \pi$. Squares: Square flux ladder (1) at $\rho = 1/4$ and $\delta = 0$, where we have fixed $\Omega = 20t$ and adjusted γ and U to match the corresponding values of t_2/t_1 and $U/|t_1|$. All quantities are extracted via finite-size extrapolation using system lengths up to $L = 120$ ($L = 80$) for the triangular (square) ladder model. Only the central half of the sites is used to compute the expected values. (b) Phase diagram of the semisynthetic square flux ladder (1) at $\rho = 1/4$ for $\Omega = 20t$ and $\delta = 0$. Black circles: Phase boundary from DMRG simulations. Blue triangles: Set of points where $U = 10t\cos(\gamma/2) = 10|t_1|$ and the effective triangular ladder (2) tunneling ratio $|t_2/t_1|$ takes values from 0.9 to 0.1, corresponding to the curves of (a).

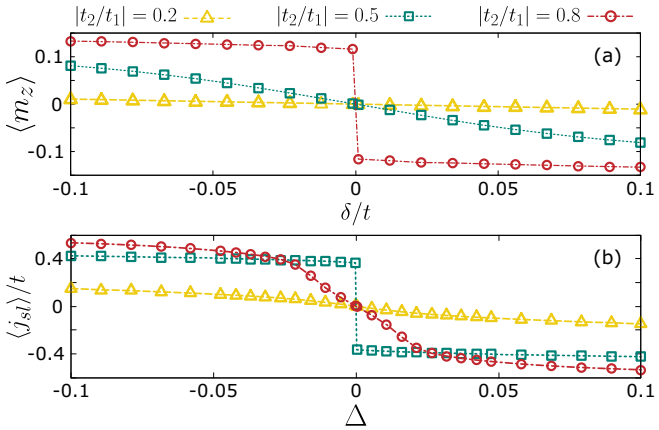

FIG. 3. (a) Magnetization m_z as a function of the Raman detuning δ, for the ground state of Hamiltonian (1) at $\rho = 1/4$, with $\Omega = 10t$ and adjusting γ and U so that $U = 10|t_1|$ and $|t_2/t_1| = 0.2$ (yellow triangles), 0.5 (teal squares), 0.8 (dark red circles), with $t_1 < 0$. (b) Staggered leg current j_{sl} defined in (5) as a function of the lattice dimerization Δ. All quantities are extrapolated to the thermodynamic limit by considering system sizes up to $L = 80$.

to the CSF of the spin chain appears when $|t_2/t_1|$ is further increased. It is characterized by the long-range order of k^2, signaling the interleg population imbalance of the BLP-SF phase [see (6)].

Figure 2(b) shows the phase diagram of the square flux ladder in the U-γ plane for $\Omega = 20t$. The blue triangles fix the condition $U = 10t \cos\gamma/2 = 10|t_1|$, and correspond to the curves displayed in Fig. 2(a). Remarkably, the three phases predicted by the effective frustrated XX model persist in wide regions of parameter space. For stronger interactions—where the truncation to the lower band is no longer accurate—a charge density wave phase (not displayed here) has been shown to appear [73,74], while the M-SF survives to the HCB limit of the flux ladder at quarter filling [75].

Finally, we numerically assess the protocol described above to probe the three phases in the square flux ladder. Figure 3(a) shows the mean magnetization m_z of the ground state as a function of δ for $\Omega = 10t$. We adjust γ to different values of $|t_2/t_1|$ and keep $U = 10|t_1|$. For $|t_2/t_1| = 0.8$, the discontinuity in m_z around $\delta = 0$ signals the spontaneous breaking of the Z_2 parity symmetry that characterizes the BLP-SF (CSF) phase. Similarly, Fig. 3(b) shows the expected value of the staggered leg current j_{sl} [see Eq. (5)] as a function of Δ. As expected, for $|t_2/t_1| = 0.5$, the spontaneous dimerization that characterizes the $\mathrm{VL}_{1/2}$-MI (BOW) is signaled by the discontinuity of j_{sl} around $\Delta = 0$.

Experimental implementation. The flux-ladder model discussed above can be implemented using a Raman-coupled Bose gas in a 1D optical lattice. This approach allows realizing large rung couplings along the synthetic direction with low Raman intensities that ensure small heating rates [18]. For concreteness, we focus on ^{41}K atoms at large magnetic fields, where the low sensitivity of δ to magnetic field fluctuations [76] provides a fine control of the effective staggered flux Φ. However, our scheme can be implemented equivalently with ^{87}Rb atoms using dynamical decoupling schemes [77,78]. We consider a blue-detuned retroreflected 1D lattice of wavelength $\lambda_{L,s} = 532$ nm of depth $5E_{L,s}$ for the physics, and an additional retroreflected lattice of wavelength $\lambda_{L,l} = 1064$ nm overlapped with it for preparing the required $\rho = 1/4$ filling and for dimerizing the system in the symmetry breaking measurements of Fig. 3 [52]. Using two Raman beams at the tune-out wavelength 769 nm and forming a $\sim 45^\circ$ angle with the lattice beams yields the required flux $\gamma \sim \pi$ [16]. In such conditions, the BOW and CSF regimes of the effective triangular model can be realized with tunneling rates $|t_{1,2}|/h$ above 100 Hz, while reaching the strongly interacting regime $U = 10|t_1|$ by confining the gas along the transverse directions with two 1064-nm perpendicular optical lattices of depth $\sim 45E_{L,l}$. Moreover, the Raman coupling $\Omega \sim 10t$ remains sufficiently large to satisfy the lower-band approximation, while enabling gas lifetimes much larger than the tunneling timescales of the effective model [52]. Finally, the magnetization and staggered leg currents of Fig. 3 can be simply determined by measuring the atomic spin populations and leg currents using a combination of Stern-Gerlach, superlattice, and time-of-flight techniques [14,18]. Thus, our proposal is immediately accessible in current experiments.

Conclusion. We have shown that semisynthetic flux ladders enable the experimental realization of a frustrated XX Heisenberg model with bosons in lattices without real geometric frustration. Our scheme is robust and does not suffer from the heating limitations of Floquet-engineering or higher-band schemes [39,40,79]. Its tunability makes it ideal for detecting multipartite entanglement [80], and for studying transport, out-of-equilibrium, and thermal [81] properties, which are challenging for classical numerical simulations but start to be accessible experimentally [24]. Whether such effective low-energy dressed-state descriptions can be successfully applied to spin models implemented in other experimental platforms [82–90], or extended to engineer 2D frustrated models with [38] or without [91] geometric frustration is an open question worth investigating.

Acknowledgments. We are grateful to C. S. Chisholm and A. Rubio-Abadal for a critical reading of the manuscript. L.B. acknowledges M. Aidelsburger, N. Baldelli, and C. R. Cabrera for discussions on related topics. Research at ICFO was supported by EU Quantum Flagship (PASQuanS2.1, Grant No. 101113690), Spanish MCIN/AEI/10.13039/501100011033 Severo Ochoa program for Centres of Excellence in R&D (CEX2019-000910-S/10.13039/501100011033) and MCIN Recovery, Transformation and Resilience Plan with funding from European Union NextGenerationEU (PRTR C17.I1), Fundació Privada Cellex, Fundació Mir-Puig, and Generalitat de Catalunya (CERCA program). L.B. acknowledges funding from Politecnico di Torino, starting package Grant No. 54 RSG21BL01 and from the Italian MUR (PRIN DiQut Grant No. 2022523NA7). L.B. and M.L. acknowledge funding from European Union (ERC AdG-833801 NOQIA, EU Horizon 2020 FET-OPEN OPTO-Logic (Grant No. 899794), and EU Horizon Europe NeQST (Grant No. 101080086)), Spanish AEI/MCIN/10.13039/501100011033 (FIDEUA PID2019-106901GB-I00, PGC2018-097027-B-I00, and QUSPIN RTC2019-007196-7), EU QUANTERA MAQS (funded by State Research Agency MICN/AEI/10.13039/501100011033, PCI2019-111828-2), Generalitat de Catalunya (AGAUR

2021 SGR 01452), Barcelona Supercomputing Center MareNostrum (FI-2022-1-0042 and FI-2023-1-0013), and the Polish National Science Centre (Symfonia Grant No. 2016/20/W/ST4/00314). L.T. acknowledges funding from European Union (ERC CoG-101003295 SuperComp), Spanish MCIN/AEI/10.13039/501100011033 (LIGAS PID2020-112687GB-C21), Deutsche Forschungsgemeinschaft (Research Unit FOR2414, Project No. 277974659), and Generalitat de Catalunya (AGAUR 2021 SGR 01448). Research at UAB was supported by MCIN/AEI/10.13039/501100011033 (LIGAS PID2020-112687GB-C22) and Generalitat de Catalunya (AGAUR 2021 SGR 00138). A.C. acknowledges support from the UAB Talent Research program. All authors acknowledge funding from EU QUANTERA DYNAMITE (funded by MICN/AEI/10.13039/501100011033 and by the European Union NextGenerationEU/PRTR PCI2022-132919 (Grant No. 101017733)), from Generalitat de Catalunya (QuantumCAT U16-011424, co-funded by ERDF Operational Program of Catalonia 2014-2020), from the Ministry of Economic Affairs and Digital Transformation of the Spanish Government through the QUANTUM ENIA project call Quantum Spain project, and by the European Union through the Recovery, Transformation and Resilience Plan NextGenerationEU within the framework of the Digital Spain 2026 Agenda.

[1] P. Anderson, Resonating valence bonds: A new kind of insulator? Mater. Res. Bull. **8**, 153 (1973).

[2] L. Balents, Spin liquids in frustrated magnets, Nature (London) **464**, 199 (2010).

[3] C. Lacroix, P. Mendels, and F. Mila, *Introduction to Frustrated Magnetism* (Springer, Berlin, 2011).

[4] H. T. Diep, *Frustrated Spin Systems* (World Scientific, Singapore, 2004).

[5] T. Senthil, A. Vishwanath, L. Balents, S. Sachdev, and M. P. Fisher, Deconfined quantum critical points, Science **303**, 1490 (2004).

[6] A. W. Sandvik, Evidence for deconfined quantum criticality in a two-dimensional Heisenberg model with four-spin interactions, Phys. Rev. Lett. **98**, 227202 (2007).

[7] S. Jiang and O. Motrunich, Ising ferromagnet to valence bond solid transition in a one-dimensional spin chain: Analogies to deconfined quantum critical points, Phys. Rev. B **99**, 075103 (2019).

[8] A. Rahmani, A. E. Feiguin, and C. D. Batista, Anyonic liquids in nearly saturated spin chains, Phys. Rev. Lett. **113**, 267201 (2014).

[9] C. Majumdar and D. Ghosh, On next-nearest-neighbor interaction in linear chain. I, J. Math. Phys. **10**, 1388 (1969).

[10] F. D. M. Haldane, Spontaneous dimerization in the $S = \frac{1}{2}$ Heisenberg antiferromagnetic chain with competing interactions, Phys. Rev. B **25**, 4925 (1982).

[11] K. Okamoto and K. Nomura, Fluid-dimer critical point in $S = 1/2$ antiferromagnetic Heisenberg chain with next nearest neighbor interactions, Phys. Lett. A **169**, 433 (1992).

[12] S. R. White and I. Affleck, Dimerization and incommensurate spiral spin correlations in the zigzag spin chain: Analogies to the Kondo lattice, Phys. Rev. B **54**, 9862 (1996).

[13] A. A. Nersesyan, A. O. Gogolin, and F. H. L. Eßler, Incommensurate spin correlations in spin-1/2 frustrated two-leg Heisenberg ladders, Phys. Rev. Lett. **81**, 910 (1998).

[14] M. Atala, M. Aidelsburger, M. Lohse, J. T. Barreiro, B. Paredes, and I. Bloch, Observation of chiral currents with ultracold atoms in bosonic ladders, Nat. Phys. **10**, 588 (2014).

[15] M. E. Tai, A. Lukin, M. Rispoli, R. Schittko, T. Menke, D. Borgnia, P. M. Preiss, F. Grusdt, A. M. Kaufman, and M. Greiner, Microscopy of the interacting Harper–Hofstadter model in the two-body limit, Nature (London) **546**, 519 (2017).

[16] A. Celi, P. Massignan, J. Ruseckas, N. Goldman, I. Spielman, G. Juzeliūnas, and M. Lewenstein, Synthetic gauge fields in synthetic dimensions, Phys. Rev. Lett. **112**, 043001 (2014).

[17] M. Mancini, G. Pagano, G. Cappellini, L. Livi, M. Rider, J. Catani, C. Sias, P. Zoller, M. Inguscio, M. Dalmonte, and L. Fallani, Observation of chiral edge states with neutral fermions in synthetic Hall ribbons, Science **349**, 1510 (2015).

[18] B. K. Stuhl, H.-I. Lu, L. M. Aycock, D. Genkina, and I. B. Spielman, Visualizing edge states with an atomic Bose gas in the quantum Hall regime, Science **349**, 1514 (2015).

[19] L. F. Livi, G. Cappellini, M. Diem, L. Franchi, C. Clivati, M. Frittelli, F. Levi, D. Calonico, J. Catani, M. Inguscio, and L. Fallani, Synthetic dimensions and spin-orbit coupling with an optical clock transition, Phys. Rev. Lett. **117**, 220401 (2016).

[20] S. Kolkowitz, S. L. Bromley, T. Bothwell, M. L. Wall, G. E. Marti, A. Koller, X. Zhang, A. M. Rey, and J. Ye, Spin–orbit-coupled fermions in an optical lattice clock, Nature (London) **542**, 66 (2017).

[21] J. H. Han, J. H. Kang, and Y. Shin, Band gap closing in a synthetic Hall tube of neutral fermions, Phys. Rev. Lett. **122**, 065303 (2019).

[22] C.-H. Li, Y. Yan, S.-W. Feng, S. Choudhury, D. B. Blasing, Q. Zhou, and Y. P. Chen, Bose-Einstein condensate on a synthetic topological Hall cylinder, PRX Quantum **3**, 010316 (2022).

[23] R. P. Anderson, D. Trypogeorgos, A. Valdés-Curiel, Q.-Y. Liang, J. Tao, M. Zhao, T. Andrijauskas, G. Juzeliūnas, and I. B. Spielman, Realization of a deeply subwavelength adiabatic optical lattice, Phys. Rev. Res. **2**, 013149 (2020).

[24] T.-W. Zhou, G. Cappellini, D. Tusi, L. Franchi, J. Parravicini, C. Repellin, S. Greschner, M. Inguscio, T. Giamarchi, M. Filippone, J. Catani, and L. Fallani, Observation of universal Hall response in strongly interacting Fermions, Science **381**, 427 (2023).

[25] S.-L. Drechsler, O. Volkova, A. N. Vasiliev, N. Tristan, J. Richter, M. Schmitt, H. Rosner, J. Málek, R. Klingeler, A. A. Zvyagin, and B. Büchner, Frustrated cuprate route from antiferromagnetic to ferromagnetic spin-$\frac{1}{2}$ Heisenberg chains: Li_2ZrCuO_4 as a missing link near the quantum critical point, Phys. Rev. Lett. **98**, 077202 (2007).

[26] C. de Graaf, I. de P. R. Moreira, F. Illas, O. Iglesias, and A. Labarta, Magnetic structure of Li_2CuO_2: From *ab initio* calculations to macroscopic simulations, Phys. Rev. B **66**, 014448 (2002).

[27] A. U. B. Wolter, F. Lipps, M. Schäpers, S.-L. Drechsler, S. Nishimoto, R. Vogel, V. Kataev, B. Büchner, H. Rosner, M. Schmitt, M. Uhlarz, Y. Skourski, J. Wosnitza, S. Süllow, and K. C. Rule, Magnetic properties and exchange integrals of the frustrated chain cuprate linarite $PbCuSO_4(OH)_2$, Phys. Rev. B **85**, 014407 (2012).

[28] H.-J. Grafe, S. Nishimoto, M. Iakovleva, E. Vavilova, L. Spillecke, A. Alfonsov, M.-I. Sturza, S. Wurmehl, H. Nojiri, H. Rosner, J. Richter, U. K. Rößler, S.-L. Drechsler, V. Kataev, and B. Büchner, Signatures of a magnetic field-induced unconventional nematic liquid in the frustrated and anisotropic spin-chain cuprate $LiCuSbO_4$, Sci. Rep. **7**, 6720 (2017).

[29] A. Orlova, E. L. Green, J. M. Law, D. I. Gorbunov, G. Chanda, S. Krämer, M. Horvatić, R. K. Kremer, J. Wosnitza, and G. L. J. A. Rikken, Nuclear magnetic resonance signature of the spin-nematic phase in $LiCuVO_4$ at high magnetic fields, Phys. Rev. Lett. **118**, 247201 (2017).

[30] H. Ueda, S. Onoda, Y. Yamaguchi, T. Kimura, D. Yoshizawa, T. Morioka, M. Hagiwara, M. Hagihala, M. Soda, T. Masuda, T. Sakakibara, K. Tomiyasu, S. Ohira-Kawamura, K. Nakajima, R. Kajimoto, M. Nakamura, Y. Inamura, N. Reynolds, M. Frontzek, J. S. White *et al.*, Emergent spin-1 Haldane gap and ferroelectricity in a frustrated spin-$\frac{1}{2}$ ladder, Phys. Rev. B **101**, 140408 (2020).

[31] C. P. Grams, D. Brüning, S. Kopatz, T. Lorenz, P. Becker, L. Bohatý, and J. Hemberger, Observation of chiral solitons in $LiCuVO_4$, Commun. Phys. **5**, 37 (2022).

[32] L. Tarruell, D. Greif, T. Uehlinger, G. Jotzu, and T. Esslinger, Creating, moving and merging Dirac points with a Fermi gas in a tunable honeycomb lattice, Nature (London) **483**, 302 (2012).

[33] J. Yang, L. Liu, J. Mongkolkiattichai, and P. Schauss, Site-resolved imaging of ultracold fermions in a triangular-lattice quantum gas microscope, PRX Quantum **2**, 020344 (2021).

[34] Z. Z. Yan, B. M. Spar, M. L. Prichard, S. Chi, H.-T. Wei, E. Ibarra-García-Padilla, K. R. A. Hazzard, and W. S. Bakr, Two-dimensional programmable tweezer arrays of fermions, Phys. Rev. Lett. **129**, 123201 (2022).

[35] A. Mazurenko, C. S. Chiu, G. Ji, M. F. Parsons, M. Kanász-Nagy, R. Schmidt, F. Grusdt, E. Demler, D. Greif, and M. Greiner, A cold-atom Fermi–Hubbard antiferromagnet, Nature (London) **545**, 462 (2017).

[36] J. Mongkolkiattichai, L. Liu, D. Garwood, J. Yang, and P. Schauss, Quantum gas microscopy of a geometrically frustrated Hubbard system, arXiv:2210.14895.

[37] A. Eckardt, P. Hauke, P. Soltan-Panahi, C. Becker, K. Sengstock, and M. Lewenstein, Frustrated quantum antiferromagnetism with ultracold bosons in a triangular lattice, Europhys. Lett. **89**, 10010 (2010).

[38] A. Celi, T. Grass, A. J. Ferris, B. Padhi, D. Raventós, J. Simonet, K. Sengstock, and M. Lewenstein, Modified spin-wave theory and spin-liquid behavior of cold bosons on an inhomogeneous triangular lattice, Phys. Rev. B **94**, 075110 (2016).

[39] J. Struck, C. Ölschläger, R. Le Targat, P. Soltan-Panahi, A. Eckardt, M. Lewenstein, P. Windpassinger, and K. Sengstock, Quantum simulation of frustrated classical magnetism in triangular optical lattices, Science **333**, 996 (2011).

[40] J. Struck, M. Weinberg, C. Ölschläger, P. Windpassinger, J. Simonet, K. Sengstock, R. Höppner, P. Hauke, A. Eckardt, M. Lewenstein, and L. Mathey, Engineering Ising-XY spin-models in a triangular lattice using tunable artificial gauge fields, Nat. Phys. **9**, 738 (2013).

[41] M. Aidelsburger, M. Atala, S. Nascimbène, S. Trotzky, Y.-A. Chen, and I. Bloch, Experimental realization of strong effective magnetic fields in an optical lattice, Phys. Rev. Lett. **107**, 255301 (2011).

[42] M. Aidelsburger, M. Atala, M. Lohse, J. T. Barreiro, B. Paredes, and I. Bloch, Realization of the Hofstadter Hamiltonian with ultracold atoms in optical lattices, Phys. Rev. Lett. **111**, 185301 (2013).

[43] H. Miyake, G. A. Siviloglou, C. J. Kennedy, W. C. Burton, and W. Ketterle, Realizing the Harper Hamiltonian with laser-assisted tunneling in optical lattices, Phys. Rev. Lett. **111**, 185302 (2013).

[44] C. Weitenberg and J. Simonet, Tailoring quantum gases by Floquet engineering, Nat. Phys. **17**, 1342 (2021).

[45] O. Boada, A. Celi, J. I. Latorre, and M. Lewenstein, Quantum simulation of an extra dimension, Phys. Rev. Lett. **108**, 133001 (2012).

[46] E. Anisimovas, M. Račiūnas, C. Sträter, A. Eckardt, I. B. Spielman, and G. Juzeliūnas, Semisynthetic zigzag optical lattice for ultracold bosons, Phys. Rev. A **94**, 063632 (2016).

[47] D. Suszalski and J. Zakrzewski, Different lattice geometries with a synthetic dimension, Phys. Rev. A **94**, 033602 (2016).

[48] J. Cabedo, J. Claramunt, J. Mompart, V. Ahufinger, and A. Celi, Effective triangular ladders with staggered flux from spin-orbit coupling in 1D optical lattices, Eur. Phys. J. D **74**, 123 (2020).

[49] M. Mamaev, I. Kimchi, R. M. Nandkishore, and A. M. Rey, Tunable-spin-model generation with spin-orbit-coupled fermions in optical lattices, Phys. Rev. Res. **3**, 013178 (2021).

[50] M. Mamaev, T. Bilitewski, B. Sundar, and A. M. Rey, Resonant dynamics of strongly interacting SU(n) fermionic atoms in a synthetic flux ladder, PRX Quantum **3**, 030328 (2022).

[51] M. Sato, S. Furukawa, S. Onoda, and A. Furusaki, Competing phases in spin-$1/2J_1$-J_2 chain with easy-plane anisotropy, Mod. Phys. Lett. B **25**, 901 (2011).

[52] See Supplemental Material at http://link.aps.org/supplemental/10.1103/PhysRevResearch.5.L042008 for a detailed derivation of the lower-band model, a discussion of its symmetry-broken phases and meaningful observables, and of the experimental viability of our proposal, which includes Refs. [53–60].

[53] Y.-J. Lin, K. Jiménez-García, and I. B. Spielman, Spin–orbit-coupled Bose–Einstein condensates, Nature (London) **471**, 83 (2011).

[54] C. K. Majumdar, Antiferromagnetic model with known ground state, J. Phys. C: Solid State Phys. **3**, 911 (1970).

[55] S. Greschner, M. Piraud, F. Heidrich-Meisner, I. P. McCulloch, U. Schollwöck, and T. Vekua, Spontaneous increase of magnetic flux and chiral-current reversal in bosonic ladders: Swimming against the tide, Phys. Rev. Lett. **115**, 190402 (2015).

[56] M. Di Dio, S. De Palo, E. Orignac, R. Citro, and M.-L. Chiofalo, Persisting Meissner state and incommensurate phases of hard-core boson ladders in a flux, Phys. Rev. B **92**, 060506 (2015).

[57] A. Frölian, Simulating a topological gauge theory in a Raman-dressed Bose-Einstein condensate, Ph.D. thesis, Universitat Politècnica de Catalunya, 2022, http://hdl.handle.net/2117/367335.

[58] R. Wei and E. J. Mueller, Magnetic-field dependence of Raman coupling in alkali-metal atoms, Phys. Rev. A **87**, 042514 (2013).
[59] A. Frölian, C. S. Chisholm, E. Neri, C. R. Cabrera, R. Ramos, A. Celi, and L. Tarruell, Realizing a 1D topological gauge theory in an optically dressed BEC, Nature (London) **608**, 293 (2022).
[60] D. Wei, A. Rubio-Abadal, B. Ye, F. Machado, J. Kemp, K. Srakaew, S. Hollerith, J. Rui, S. Gopalakrishnan, N. Y. Yao, I. Bloch, and J. Zeiher, Quantum gas microscopy of Kardar-Parisi-Zhang superdiffusion, Science **376**, 716 (2022).
[61] S. Greschner, L. Santos, and T. Vekua, Ultracold bosons in zigzag optical lattices, Phys. Rev. A **87**, 033609 (2013).
[62] M. P. Zaletel, S. A. Parameswaran, A. Rüegg, and E. Altman, Chiral bosonic Mott insulator on the frustrated triangular lattice, Phys. Rev. B **89**, 155142 (2014).
[63] C. Romen and A. M. Läuchli, Chiral Mott insulators in frustrated Bose-Hubbard models on ladders and two-dimensional lattices: A combined perturbative and density matrix renormalization group study, Phys. Rev. B **98**, 054519 (2018).
[64] S. Greschner and T. Mishra, Interacting bosons in generalized zigzag and railroad-trestle models, Phys. Rev. B **100**, 144405 (2019).
[65] C.-M. Halati and T. Giamarchi, Bose-Hubbard triangular ladder in an artificial gauge field, Phys. Rev. Res. **5**, 013126 (2023).
[66] T. Mishra, R. V. Pai, S. Mukerjee, and A. Paramekanti, Quantum phases and phase transitions of frustrated hard-core bosons on a triangular ladder, Phys. Rev. B **87**, 174504 (2013).
[67] T. Mishra, R. V. Pai, and S. Mukerjee, Supersolid in a one-dimensional model of hard-core bosons, Phys. Rev. A **89**, 013615 (2014).
[68] E. Orignac and T. Giamarchi, Meissner effect in a bosonic ladder, Phys. Rev. B **64**, 144515 (2001).
[69] R. Wei and E. J. Mueller, Theory of bosons in two-leg ladders with large magnetic fields, Phys. Rev. A **89**, 063617 (2014).
[70] A. Tokuno and A. Georges, Ground states of a Bose–Hubbard ladder in an artificial magnetic field: Field-theoretical approach, New J. Phys. **16**, 073005 (2014).
[71] S. R. White, Density matrix formulation for quantum renormalization groups, Phys. Rev. Lett. **69**, 2863 (1992).
[72] M. Fishman, S. R. White, and E. M. Stoudenmire, The ITensor software library for tensor network calculations, SciPost Phys. Codebases 4 (2022).
[73] M. Piraud, F. Heidrich-Meisner, I. P. McCulloch, S. Greschner, T. Vekua, and U. Schollwöck, Vortex and Meissner phases of strongly interacting bosons on a two-leg ladder, Phys. Rev. B **91**, 140406 (2015).
[74] S. Greschner, M. Piraud, F. Heidrich-Meisner, I. P. McCulloch, U. Schollwöck, and T. Vekua, Symmetry-broken states in a system of interacting bosons on a two-leg ladder with a uniform Abelian gauge field, Phys. Rev. A **94**, 063628 (2016).
[75] A. Petrescu and K. Le Hur, Bosonic Mott insulator with Meissner currents, Phys. Rev. Lett. **111**, 150601 (2013).
[76] M. Buser, C. Hubig, U. Schollwöck, L. Tarruell, and F. Heidrich-Meisner, Interacting bosonic flux ladders with a synthetic dimension: Ground-state phases and quantum quench dynamics, Phys. Rev. A **102**, 053314 (2020).
[77] D. Trypogeorgos, A. Valdés-Curiel, N. Lundblad, and I. B. Spielman, Synthetic clock transitions via continuous dynamical decoupling, Phys. Rev. A **97**, 013407 (2018).
[78] R. P. Anderson, M. J. Kewming, and L. D. Turner, Continuously observing a dynamically decoupled spin-1 quantum gas, Phys. Rev. A **97**, 013408 (2018).
[79] X.-Q. Wang, G.-Q. Luo, J.-Y. Liu, G.-H. Huang, Z.-X. Li, C. Wu, A. Hemmerich, and Z.-F. Xu, Observation of nematic orbital superfluidity in a triangular optical lattice, arXiv:2211.05578.
[80] S. Singha Roy, L. Carl, and P. Hauke, Genuine multipartite entanglement in a one-dimensional Bose-Hubbard model with frustrated hopping, Phys. Rev. B **106**, 195158 (2022).
[81] M. Buser, F. Heidrich-Meisner, and U. Schollwöck, Finite-temperature properties of interacting bosons on a two-leg flux ladder, Phys. Rev. A **99**, 053601 (2019).
[82] S. de Léséleuc, V. Lienhard, P. Scholl, D. Barredo, S. Weber, N. Lang, H. P. Büchler, T. Lahaye, and A. Browaeys, Observation of a symmetry-protected topological phase of interacting bosons with Rydberg atoms, Science **365**, 775 (2019).
[83] V. Lienhard, P. Scholl, S. Weber, D. Barredo, S. de Léséleuc, R. Bai, N. Lang, M. Fleischhauer, H. P. Büchler, T. Lahaye, and A. Browaeys, Realization of a density-dependent peierls phase in a synthetic, spin-orbit coupled Rydberg system, Phys. Rev. X **10**, 021031 (2020).
[84] T. Graß, C. Muschik, A. Celi, R. W. Chhajlany, and M. Lewenstein, Synthetic magnetic fluxes and topological order in one-dimensional spin systems, Phys. Rev. A **91**, 063612 (2015).
[85] Y. Shapira, T. Manovitz, N. Akerman, A. Stern, and R. Ozeri, Quantum simulations of interacting systems with broken time-reversal symmetry, arXiv:2205.11178v1.
[86] A. V. Gorshkov, S. R. Manmana, G. Chen, J. Ye, E. Demler, M. D. Lukin, and A. M. Rey, Tunable superfluidity and quantum magnetism with ultracold polar molecules, Phys. Rev. Lett. **107**, 115301 (2011).
[87] J. L. Bohn, A. M. Rey, and J. Ye, Cold molecules: Progress in quantum engineering of chemistry and quantum matter, Science **357**, 1002 (2017).
[88] J. S. Douglas, H. Habibian, C.-L. Hung, A. V. Gorshkov, H. J. Kimble, and D. E. Chang, Quantum many-body models with cold atoms coupled to photonic crystals, Nat. Photon. **9**, 326 (2015).
[89] D. E. Chang, J. S. Douglas, A. González-Tudela, C.-L. Hung, and H. J. Kimble, Colloquium: Quantum matter built from nanoscopic lattices of atoms and photons, Rev. Mod. Phys. **90**, 031002 (2018).
[90] E. Colella, A. Kosior, F. Mivehvar, and H. Ritsch, Open quantum system simulation of faraday's induction law via dynamical instabilities, Phys. Rev. Lett. **128**, 070603 (2022).
[91] M. Di Liberto and N. Goldman, Chiral orbital order of interacting bosons without higher bands, Phys. Rev. Res. **5**, 023064 (2023).